Citation: Balzter, H. (2001): Forest mapping and monitoring with interferometric Synthetic Aperture Radar (InSAR). Progress in Physical Geography 25, 159-177.

Forest mapping and monitoring with interferometric Synthetic Aperture Radar (InSAR)

BALZTER, Heiko

Address for correspondence:
Heiko Balzter
Centre for Ecology and Hydrology
Institute of Terrestrial Ecology
Section for Earth Observation
Monks Wood
Abbots Ripton
Huntingdon
Cambridgeshire
PE28 2LS
UK
Tel +44 (0) 1487 77 2471
Fax +44 (0) 1487 77 3277
E-mail: hbal@ceh.ac.uk

Keywords

biomass, stem volume, forest structure, fire scars, deforestation, freeze-thaw transition, tree height, land cover mapping, SAR

Abstract

A Synthetic Aperture Radar (SAR) is an active sensor transmitting pulses of polarized electromagnetic waves and receiving the backscattered radiation. SAR sensors at different wavelengths and with different polarimetric capabilities are being used in remote sensing of the Earth. The value of an analysis of backscattered energy alone is limited due to ambiguities in the possible ecological factor configurations causing the signal. From two SAR images taken from similar viewing positions with a short time-lag, interference between the two waves can be observed. By subtracting the two phases of the signals, it is feasible to eliminate the random contribution of the scatterers to the phase. The interferometric correlation and the interferometric phase contain additional information on the three-dimensional structure of the scattering elements in the imaged area.

A brief review of SAR sensors is given, followed by an outline of the physical foundations of SAR interferometry and the practical data processing steps involved. An overview of applications of InSAR to forest mapping and monitoring is given, covering tree bole volume and biomass, forest types and land cover, fire scars, forest thermal state and forest canopy

height.

I Introduction

Remote sensing of forests has an important role in mapping large forest tracts that are difficult to access on the ground, and in monitoring changes in these forests. The forest canopy is characterised by different vegetation layers, like weeds, shrubs, undergrowth and different tree canopy layers. Optical sensors can only detect the upper canopy, where the absorption and reflection of parts of the spectrum of visible light and infrared is taking place. Therefore, radar sensors have widely been used for large-scale forest mapping. A radar operates in the microwave spectrum at wavelengths typically between 3 and 25 cm, much longer than visible light. The sensor actively transmits pulses of electromagnetic energy and receives the response from the imaged area. Because of the longer wavelength, the radiation penetrates the top vegetation layer to a certain extent and is scattered by stems, branches, twigs, leaves or needles. Microwaves also enable a weather- and illumination-independent imaging process: They can penetrate clouds, dry snow and to some extent rain. Virtually no part of the Earth's surface is permanently covered with rain of sufficient intensity to cause major difficulties. Observations can be made at day and night, for instance throughout the winter darkness of the polar regions.

Analysis of the data produced by Synthetic Aperture Radar (SAR) sensors can be used to provide estimates of parameters such as forest area, forest thermal state (frozen / thawed), forest biomass density and tree height. Such studies have been conducted over a wide range

of climate zones but more recently have been concentrated on the boreal forests of North America and Eurasia. This article gives an introduction to the imaging process, available SAR systems and the different areas of application of interferometric SAR to forest mapping. Polarimetric SAR is only covered if it is also interferometric. A wide range of references concerning the use of conventional SAR (i.e. backscatter at one wavelength and polarization) is deliberately not covered here.

II Synthetic Aperture Radar

1 Sensor characteristics

A radar sensor transmits pulses of electromagnetic radiation in the microwave spectrum. When the radiation hits an object, the electromagnetic wave is scattered and a fraction of it is reflected in the direction of the sensor. The amount of radiation received by the sensor is called radar backscatter. In contrast to Real Aperture Radar systems, Synthetic Aperture Radar (SAR) makes use of the Doppler effect of the aircraft or satellite motion to increase the resolution of the images. A SAR is a coherent imaging sensor measuring both real and imaginary components of the backscattered signal. A sensor is mainly characterised by the wavelength (or frequency), polarization, range and azimuth resolution. Operational radar wavelengths used for forest mapping are X-band (3.1 or 3.5 cm wavelength), C-band (5.65 cm), L-band (24 cm) and P-band (30-60 cm). Important platform features are the available swath widths and the repeat cycle. Longer wavelengths tend to penetrate deeper into the

vegetation canopy. The sensor transmits a polarized wave. If the electrical field of the electromagnetic wave oscillates horizontally, the transmitted wave is horizontally (H) polarized. Vertical (V) polarization is defined in the same way. Dual-polarization sensors can transmit and receive in both polarizations, but only quad-polarized (fully polarimetric) sensors record the whole polarization vector of the backscattered signal.

The backscattered intensity is higher for vegetated areas than for bare soil, because of the multiple scattering in the vegetation layer. From calm water surfaces, the backscatter is very low, as most of the radiation is reflected from the water surface away from the sensor.

The magnitude of microwave backscatter is a result of the geometric and dielectric properties of the surfaces or volumes imaged. It is sensitive to the surface geometry (topography), surface roughness (surface slope, variation of surface height, plant geometry) and water content of surface materials (crop and soil moisture, snow wetness).

The received backscatter in one pixel is the spatial sum of radar echoes of all scatterers within the imaged area on the ground. Adding up electromagnetic waves with different phases may result in constructive and destructive interference. Constructive interference means that the amplitude of the resulting radar echo is larger than that of the interacting waves, and destructive interference means that the resulting amplitude is smaller. This phenomenon is called “speckle” and causes SAR images to look like “salt and pepper”. To improve the accuracy of the backscatter estimation, backscatter values of adjacent pixels in the single-look image are averaged. This process of multi-looking improves the radiometric resolution at the expense of spatial resolution. It changes the distribution function of the backscattered power.

2 Airborne and spaceborne SAR sensors

Five spaceborne imaging radars systems were until recently or are currently in operation, ERS-1, JERS-1 (terminated in October 1998), SIR-C (operated for two 10 day periods during 1994), ERS-2 and Radarsat. Missions planned for the near future include the European ENVISAT and the Japanese ALOS satellites. Details of these systems are shown in Table 1. The suitability of a SAR sensor for interferometric purposes requires a well calibrated phase (Freeman 1992).

• The European Research Satellite - 1 (ERS-1) is the first of two identical polar orbiting Earth-viewing satellites launched by the European Space Agency (ESA). The imaging radar is C-band (5.7 cm wavelength or a frequency of 5.25 GHz) with vertical transmit and vertical receive (VV) polarization. It illuminates the Earth's surface at an incidence angle of 23º with a transmitted power of 4.8 kW per pulse. ERS-1 images a swath 100 km in width at a resolution of 30 m (for 4 looks). The satellite altitude ranges from 775 km, providing a 3 day repeat coverage for the winter ice phases for the commissioning phase which comprised the first 3 months of the mission, to 781 km, providing a 35 day repeat for global access, to 783 km, providing a 168 day repeat for the geodetic portion of the mission.

• ERS-2 was launched in spring 1995 into a 781 km, 35 day repeat orbit identical to ERS-1. On a number of occasions ERS-1 and ERS-2 have been operated as a one-day repeat Tandem Mission primarily for interferometric applications. In addition the ERS repeat cycle of 35 days means that interferometric measurements can also be made with a temporal repeat cycle of n*35 days. Interferometric pairs can be browsed using a software package from the European Space Agency (Delia and Biasutti 1999). Rufino et al. (1998) reported that only tandem pairs allow an efficient interferometric processing because of their sufficiently short time-lag of one day, whereas correlation adequate for differential interferometry could not be

achieved.

• ESA plans to launch a further SAR system aboard its ENVISAT satellite in 2000. As with ERS-1 and ERS-2 this will be a C-band system (though at a slightly different frequency which precludes ENVISAT/ERS-2 interferometry). The advanced SAR (ASAR) will have many modes, unlike the single mode of the ERS SAR. These modes include an alternating polarization mode enabling it to transmit in horizontal or vertical polarization and receive in both. Although still not a fully quad-polarized system, it will measure the cross polarized (HV) return which is important for forestry applications. ASAR also has a ScanSAR mode which permits imaging over wider swathes at coarser resolutions. Like ERS the ENVISAT orbital repeat cycle will be 35 days, but unlike ERS for ENVISAT interferometric measurements will need to be specifically programmed into the satellite mission as a result of the flexibility of ASAR. In fact for vegetation studies at C-band a 35 day repeat cycle is likely to be of only limited use when contrasted with the 1 day Tandem Mission repeat cycle of ERS-1 / ERS-2.

• The Japanese Earth Resources Satellite - 1 (JERS-1) was launched by the National Space Development Agency of Japan (NASDA) in Summer 1992 on a 3 year mission. The characteristics of its SAR are very similar to those of NASA's Seasat satellite which laid the foundation for all later satellite SARs during its a brief 3 month mission in 1978. The JERS-1 imaging radar is L-band (20 cm wavelength or a frequency of 1.28 GHz) with horizontal transmit and horizontal receive (HH) polarization. The transmitted power of a pulse is 1.3 kW. It illuminates the Earth's surface at an incidence angle of 35º from nadir, and images a swath 75 km in width at a resolution of 18m (for 3 looks). The satellite orbital repeat cycle means that interferometry can be conducted with a repeat-cycle of n*44 days (Rossi et al. 1996). The satellite orbit was not maintained as exactly as that of ERS so that the spatial

distance between the two antenna positions was often larger, but for JERS-1 this was less critical because of the longer wavelength and the greater incidence angle. Imaging positions 5 km apart would still produce fringes in the interferogram, whereas for the ERS satellites 1.1 km is the largest antenna separation for which interferometry is theoretically possible (Rossi et al. 1996). In 1998 JERS-1 stopped transmitting data because of a failure of the solar panels. JERS-1 has been used in the Global Rain Forest Monitoring Project to make radar mosaics of the entire tropical forest belt, comprising the Amazon basin and Congo basin (both at high and low water levels), West Africa, South-East Asia, Indonesia and Papua New Guinea. Data has also been acquired in the Global Boreal Forest Monitoring Project to make similarly large scale mosaics of the entire boreal forest belt, comprising the North American forests (Alaska and Canada) and Eurasian forests (Scandinavia and Russia).

- NASDA plan to launch an Advanced Land Observation Satellite (ALOS) in 2002, which will carry a Phased Array type L-band SAR (PALSAR) capable of polarimetry and repeat-pass interferometry.
- Two radar missions are planned for the near future by NASA: The Shuttle Radar Topography Mission (SRTM) will generate a global high resolution digital elevation model from X-band single-pass interferometry in which the second antenna will be deployed at the end of a 80m boom extended from the Space Shuttle, and LightSAR will be used for the development of commercial applications. LightSAR is planned to carry an L- and an X-band antenna (Hilland et al. 1998).
- The Canadian RADARSAT satellite can observe in a number of resolution and swathe width modes including a Spotlight (high resolution) mode and a ScanSAR mode which permits imaging over swathes up to 500 km wide at a resolution of 100 m. As with Envisat, because of the flexibility of the SAR, interferometric measurements have to be specifically

programmed into the satellite mission.

• The only fully polarimetric spaceborne SAR so far was the L- and C-band system aboard SIR-C which was deployed during two 10-day missions during 1994.

• Polarimetric data are available from a number of airborne systems including JPL's TOPSAR system (Madsen et al. 1995), JPL's AIRSAR aboard a NASA DC-8, TUD-DCRS's EMISAR aboard a Danish Airforce Fanjet (Christensen et al. 1998), DLR's E-SAR aboard a Dornier 228, and more recently Dornier's DoSAR also aboard a Dornier 228. Do-SAR was the first airborne single-pass interferometric SAR in Europe (Faller and Meier 1995), and has been used to estimate terrain height with an accuracy of 2-5 m. Gray and Farrismanning (1993) studied repeat-pass interferometry with an airborne SAR. Coherence between separate images requires very accurate flightline control and very close flightpaths with offsets less than a few tens of meters. Repeat-pass interferometry with airborne SAR opens the possibility for temporal coherence studies and differential interferometric SAR experiments with the flexibility afforded by the airborne platform. As well as a direct use for programmes observing relatively small areas of the Earth, these airborne radars act as development systems for future more sophisticated satellite radars.

III SAR Interferometry

In this section, a brief introduction to the background of SAR interferometry is provided. For a thorough and detailed introduction the interested reader is referred to Bamler and Hartl (1998), and for a review of techniques and applications see Gens and Van Genderen (1996).

1 Physical background

Radar backscatter is measured as a complex number, containing information about the intensity of the signal and the phase (Figure 1). The phase is determined by the two-way path length from the sensor to the resolution cell on the ground and the interference between individual scatterers (e.g. trees) in that cell. If two complex SAR images have been acquired over the same area from very close antenna positions then the within-cell interference contribution to the phase is almost identical for both images. The temporal or spatial separation between the two antennas of the interferometric SAR signals is called the baseline. Figure 2 illustrates the viewing geometry of SAR interferometry. The phases of the two signals interfere in a characteristic pattern. The phase difference between the two images for each resolution cell is directly related to the difference between the viewing distances of the two sensors. In particular the average three-dimensional position of the scattering elements may be inferred leading to the capability to derive topographic maps from the phase difference images.

SAR backscatter intensity is strongly affected by terrain properties (slope and aspect). SAR interferometry provides a method of removing topographic effects from the backscatter without the need for additional external data sets and leaving only backscatter variations arising from changes in target parameters, such as vegetation biomass or soil moisture. The capability to derive Digital Elevation Models (DEM) also provides a vital input into mapping out drainage networks and separating water catchments, particularly in poorly surveyed areas. The two images from which an interferogram is generated can either be acquired using one

antenna for repeated passes over the same area at two different times (Repeat Pass Interferometry) or can be acquired simultaneously using two spatially separated antennas on the same platform (Single Pass Interferometry).

To compute an interferogram the two single look complex (SLC) SAR images are first co-registered to an accuracy of less than 0.1 pixel. The complex vector product is then formed on a pixel by pixel basis to derive a phase difference and a correlation at each position. The interferometric correlation is a measure of the accuracy of the estimation of the interferometric phase. A normalised interferogram is defined as the complex degree of coherence of the two complex image values s_1 and s_2 given by:

$$\gamma = \frac{< s_1 \cdot s_2 * >}{\sqrt{< s_1 \cdot s_1 * >< s_2 \cdot s_2 * >}} \qquad [1]$$

where the < > brackets represent an ensemble average, formed by coherently averaging the complex values of n single look pixels, and * represents the complex conjugate:

$$< s_1 \cdot s_2 * >= \frac{1}{n}\sum_{i=1}^{n} s_{1,i} \cdot s_{2,i} * \qquad [2]$$

Interference phenomena such as fringes will be observed so long as there is at least partial coherence between the two images. The phase of γ is the interferometric phase and the magnitude of γ is the degree of coherence between s_1 and s_2. γ represents the fringe visibility and lies within the range zero to unity. γ can be shown to be the product of three terms:

$$\gamma = |\gamma|_{noise} \cdot |\gamma|_{temporal} \cdot |\gamma|_{spatial} \qquad [3]$$

representing decorrelation arising from the system noise, from differences in the target over the temporal and over the spatial baseline (Zebker and Villasenor 1992).

$|\gamma|_{noise}$ is related to the signal to noise ratio (SNR) of the sensor, and is only significant for areas of very low backscatter:

$$|\gamma|_{noise} = \frac{1}{1+\frac{1}{SNR}} \qquad [4]$$

$|\gamma|_{spatial}$, the baseline decorrelation, arises from surface and volume scattering and can be separated as follows:

$$|\gamma|_{spatial} = |\gamma|_{slantrange} \cdot |\gamma|_{volume} \qquad [5]$$

$|\gamma|_{slantrange}$ can be increased to 1 by applying common band (spectral shift) filtering. However $|\gamma|_{volume}$ is only 1 in the case when the scatterers are confined to a plane. When they are distributed in depth, as for example with multiple scattering from a forest canopy, then there is appreciable volume decorrelation.

$|\gamma|_{temporal}$, the decorrelation of the target arising from the time separation of the two observations, is very low for stable, man-made structures, moderate for bare soil surfaces and agricultural crops and substantial for tall vegetation such as forests. In the case of vegetation targets, these temporal changes are caused by changes of the scatterers (growth or loss of

foliage, wind motion) and changes in their dielectric constant (surface moisture film, freezing, thawing). For agricultural crops the mechanical cultivation associated with farming activities such as harvesting, ploughing, mowing, and tillage causes complete decorrelation as almost all scatterers are changed.

In addition to being influenced by temporal and spatial effects, the interferometric coherence is, like the backscatter intensity, also influenced by the observing wavelength. Backscatter arises predominantly from target components on the scale of the radar wavelength. Thus in the case of a forest canopy JERS-1 L-band backscatter arises more from the trunk and branches of the trees whereas ERS C-band backscatter arises more from their twigs and leaves or needles. Since the longer wavelength scatterers are more stable, coherence tends to be maintained over a longer temporal interval at longer wavelengths. For example for a forest canopy coherence is maintained over the 44 day repeat cycle of JERS-1, but not over the 35 day repeat cycle of ERS. In the latter case image pairs from the Ice Phase with a three day repeat cycle for ERS-1 or from the Tandem Mission with one day repeat cycle for ERS-1 / ERS-2 are required to maintain coherence. In all cases the coherence or fringe visibility must be sufficient to enable the fringe phase to be derived accurately, for an error in phase translates directly into an error in height measurement.

Interferogram images derived from repeat-pass spaceborne SAR systems are known to exhibit artefacts due to the time and space variations of atmospheric water vapour. Zebker et al. (1997) therefore recommended to use the longest radar wavelengths possible and to maximise the spatial baseline within decorrelation limits. To detect surface deformation they suggest to use multiple observations and to average the InSAR derived products.

To ensure the highest coherence over vegetation targets, temporal decorrelation can be avoided completely by making the interferometric measurements almost coincident in time as well as almost coincident in space. Rather than a Repeat Pass Interferometric system, a Single

Pass Interferometric system is required - the two measurements from which the interferogram is to be generated are made from two antennas across the track. The first such system in space will be the Shuttle Radar Topographic Mission (SRTM).

Tough et al. (1995) analyse the statistical distributions of the amplitude and phase difference in single look data. However, multi-look data have completely different statistical properties, and Lee et al. (1994) examine the probability distribution functions of the multi-look phase difference, magnitude of complex product, and intensity and amplitude ratios between two components of the scattering matrix. They conclude that the distribution functions depend on the complex correlation coefficient and the number of looks.

In broad terms, SAR interferometry provides information on the spatial distribution of the scatterers which make up the target while SAR polarimetry provides information on the scattering mechanisms predominating in each target, for example surface scattering, double-bounce scattering and volume scattering. Polarimetric SAR interferometry provides information on the spatial distributions of the scattering mechanisms making up the target. In particular, the decorrelation components $|\gamma|_{spatial}$ and $|\gamma|_{temporal}$ in eq. 3 are known to be polarization-dependent (Cloude and Papathanassiou 1998).

In the case of a forest observed at L-band, where the total backscatter is made up of contributions from a number of different scattering mechanisms, the co-polarized return tends to have a substantial component arising from returns from the ground while the cross-polarized return tends to be dominated by returns from multiple scattering within the forest canopy. The vertical spatial separation of the phase scattering centres of different scattering mechanisms in the canopy provides the basis for an improved retrieval of vegetation height.

2 Interferometric processing chain

The first processing step is co-registration of the Single Look Complex (SLC) images (Lin et al. 1992; Fornaro and Franceschetti 1995; Rufino et al. 1998). To achieve a high quality interferogram, co-registration at sub-pixel accuracy is required, ideally better than 0.2 pixel, otherwise the interferometric coherence is reduced considerably. In the following step common band filtering is performed to improve coherence estimation by increasing $|\gamma|_{slantrange}$ in eq. 5.

In the second step the normalised complex interferogram is computed. The two co-registered images are multi-looked to improve estimation accuracy and then cross-correlated. The resulting interferogram consists of complex values with the magnitude corresponding to the multi-looked interferometric correlation and the phase to the interferometric phase.

The phase trends in azimuth and range direction resulting from the Earth's curvature is then removed from the interferogram (phase flattening).

To retrieve the effective height from the phase of the complex interferogram the correct multiple of 2π has to be added in the phase unwrapping step. Phase unwrapping is problematic due to fringe discontinuities caused by layover (Gelautz et al. 1996), areas of low coherence, and phase noise. Filtering and multi-looking can be used to reduce the phase noise. A review of phase unwrapping techniques is given by Griffiths and Wilkinson (1994). Phase-unwrapping is often based on Goldstein's branch-cut approach (Goldstein and Werner 1998). However, holes that are isolated by branch-cuts often remain in interferograms with high noise levels. Wang and Li (1999) present two algorithms to improve the unwrapped phase image. Just and Bamler (1994) studied the dependence of the phase bias and variance on processor parameters. Phase noise can be characterised by an additive noise model. Lee et

al. (1998) developed an adaptive filtering algorithm based on this noise model. Their algorithm can be included in an iterative phase unwrapping step. Other approaches to phase unwrapping are based on fringe detection (Lin et al. 1992), region growing (Fornaro and Sansosti 1999, Xu and Cumming 1999), weighted least squares (Pritt 1996), the finite element method (Fornaro et al. 1997a), the Green's function and the Helmholtz equation (Fornaro et al. 1996, Lyuboshenko and Maitre 1999), the fast Fourier transform (Costantini et al. 1999), the minimum cost flow on a network (Costantini 1998) and local frequency estimates (Trouve et al. 1998). Zebker and Lu (1998) present a synthesis of two frequently used phase unwrapping algorithms, the residue-cut and the least-squares techniques. Their synthesis offers greater spatial coverage with less distortion. Fornaro et al. (1997b) compared global and local phase unwrapping techniques. Bamler and Hartl (1998) discuss approaches to phase unwrapping in more detail.

After successful phase unwrapping, a height map can be derived (Madsen et al. 1993; Zebker et al. 1994a; Zebker et al. 1994b). For this step a precise baseline estimate is crucial, and a refined baseline estimation needs to be carried out with a number of ground control points of known height. Accurate baseline estimation is crucial for derivation of a height map, and the orbital state vectors may not always provide the required precision. A mathematical method for the estimation of the two-dimensional orbital shift based on the fringe pattern in the interferogram has been developed by Goyal and Verma (1996) to tackle the problem.

In the final processing step, the height values in SAR image geometry (slant range) are transformed to orthonormal coordinates.

IV Applications of InSAR to forest mapping and monitoring

1 Tree biomass and bole volume

Within NASA's Mission to Planet Earth Kasischke et al. (1997) describe the capability of imaging radars to monitor variations in biomass in forest ecosystems. Radar backscatter is increasing in a non-linear way with forest biomass. The shape of this function is known to be dependent on wavelength, polarization, forest type and moisture conditions. As Baker et al. (1994) showed for Corsican Pine stands, the cross-polarized term (horizontal transmit, vertical receive, HV) is often most strongly correlated with forest biomass. This phenomenon is caused by the depolarization of the electromagnetic waves by multiple scattering events in the canopy. At a certain biomass level, the radar signal saturates. Dobson et al. (1992) analysed radar responses at P-, L- and C-band to biomass of mono-species conifer plantations at Les Landes, France, and Duke forest, North Carolina, and found an approximately linear response of backscatter to increasing biomass with wavelength-dependent saturation levels around 200 t/ha for P-band and 100 t/ha for L-band. In the study of Imhoff (1995) saturation was reached at 100 t/ha for P-, 40 t/ha for L- and 20 t/ha for C-band in coniferous and broadleaf evergreen forests. Luckman et al. (1998) found a saturation at 60 t/ha for L-band in tropical forests. Ranson et al. (1995) used the ratio of the cross-polarized intensities at two wavelengths (L-HV / C-HV), to estimate boreal forest biomass in Canada with a 95% confidence interval of ±20 t/ha, and found that saturation was reached at 200 t/ha. The accuracy with which biophysical parameters can be retrieved from SAR measurements of forests depends considerably upon vegetation structure and ground conditions (Baker and

Luckman 1999). The upper levels of sensitivity for L-band and C-band systems such as SIR-C range between <100 t/ha for complex tropical forest canopies to 250 t/ha for simpler forests dominated by a single tree species. Best performance for biomass estimation is achieved using lower frequency (P- and L-band) radar systems with a cross- polarized (HV or VH) channel. The long wavelength is required to penetrate the upper canopy layer and interact with branches and stems. Interferometric SAR can improve biomass retrieval from radar backscatter through the interferometric information about the imaging geometry: The fringe frequencies of the interferogram can be used to correct radar backscatter intensity for terrain effects (Ulander 1996), and thus improve radiometric calibration.

The interferometric coherence is sometimes found to decrease with increasing forest biomass, but this relationship is temporally unstable and may be affected by changing weather conditions between the repeated image acquisitions, terrain effects, wind, rain, snow and moisture, freezing and thawing or the spatial baseline for different image pairs.

2 Classification of forest types and land cover

Radar provides a means to classify land-cover patterns because of its sensitivity to variations in vegetation structure and vegetation and ground-layer moisture (Kasischke et al. 1997). Like-polarized imaging radars (HH or VV) are well suited for the detection of flooding under vegetation canopies, as has been demonstrated with JERS-1 SAR for the Amazon basin. Lower frequency radars (P- and L-band) are best suited for detecting flooding under forests, whereas higher frequency radars (C- band) work best for wetlands dominated by herbaceous vegetation (Kasischke et al. 1997).

During the Shuttle Imaging Radar C (SIR-C) campaigns of April and October 1994 the orbit was tightly controlled to give baselines sufficiently short for interferometry to be conducted using data from the missions. Rignot (1996) made repeat-pass interferometric radar observations of tropical rain forest in the state of Rondonia, Brazil, and found that over the forest no coherence between the two signals was found at C-band but that at L-band coherence was maintained over the entire landscape. Similar observations were made by Rosen et al. (1996), who made coherence measurements of Kilauea volcano, Hawaii. This is caused by the different scattering mechanisms affecting the signal. Short wavelengths are scattered mostly by leaves, twigs or needles in the tree crowns, whereas longer wavelengths penetrate deeper into the canopy and are scattered by large branches and stems. Because the orientation of the leaves in the tree crown changes with wind, but the upper branches remain geometrically more or less unchanged, coherence is lost at C-band but preserved at L-band. Coltelli et al. (1996) used multifrequency repeat-pass interferometry over Mount Etna, Sicily, and found that the coherence maps allowed vegetated and unvegetated areas to be separated. Askne et al. (1997) used ERS InSAR coherence to separate forested and non-forested areas. A hierarchical unsupervised segmentation algorithm for land cover classification from multi-temporal InSAR images has been developed by Dammert et al. (1999). Wegmuller and Werner (1995) studied the potential of SAR interferometry for forest mapping and monitoring, using interferometric correlation and backscatter intensities from ERS-1 SAR repeat-pass interferometric data. Forest could be clearly discriminated from other land categories. Coherence increased from coniferous, mixed to deciduous forest. Because Wegmuller and Werner (1995) used a November image pair, the deciduous trees had shed their leaves. The branches of these deciduous winter forests act as scatterers which are more stable over time than the needles of winter-green coniferous trees. Dependencies on the spatial and temporal baselines and the seasons were also analysed. The results found for the

temperate forest site around Bern, Switzerland, were extended to a boreal forest site along the Tanana River, Alaska. Repeat-pass interferometry was found to be particularly sensitive to changes such as soil freezing, mechanical cultivation of agricultural fields, and vegetation growth. In the case of soil moisture changes and freezing, the dielectric properties change without a simultaneous geometric change so that the backscatter difference is high but the coherence is the same. To visualise the information content of the interferometric signatures Wegmuller and Werner (1995) proposed a colour-composite comprising the coherence in red, mean backscatter in green and backscatter change in blue (see image 4). In this representation different targets have readily identifyable colours, for example forests tend to appear in green (low coherence, high backscatter and little backscatter change), water in blue (low coherence, low backscatter but significant backscatter change) and bare soil areas in red (high coherence, medium backscatter and little backscatter change). In a subsequent paper Wegmuller and Werner (1997) studied the retrieval of vegetation parameters using SAR interferometry.

Based upon the interferometrically derived forest map generated above, a classification was derived and then geocoded using the interferometrically derived height map generated from the same ERS SAR data pair. From a digital forest map the remotely sensed classification was validated and mapping accuracies of over 90% were achieved. Coniferous, deciduous and mixed forest stands could be distinguished and separated from orchards, regrowth and clear-cut areas. Another example for land cover classification is given by Dutra and Huber (1999), who compared different classification algorithms for four land-cover classes of the Czech Republic from ERS InSAR imagery with an overall classification accuracy exceeding 90%.

3 Fire scars

The large volume of ERS data collected at the Canadian and Alaskan receiving stations have been used for a detailed study of high-latitude terrestrial ecosystems in North America. The SAR imagery has been used to study carbon dioxide fluxes from boreal forests, particularly the effect of boreal forest fires on the CO_2 flux and the measurement of the length of the growing season as an aid in determination of the seasonal CO_2 flux, many of these studies being parts of the BOREAS project (Moghaddam and Saatchi 1995; Ranson et al. 1995; Chang et al. 1997; Ranson et al. 1997; Way et al. 1997).

4 Forest thermal state

In boreal forests the summer frost-free period bounds the growing season length for coniferous forest species and the period of root and soil respiration and decomposition in the broader landscape, while for both coniferous and deciduous forest species the growth potential is further limited by their capability for mineral and water uptake. In studying the seasonal dynamics of the boreal forest ecosystem the onset and duration of favourable soil temperatures is therefore as important as the temperature regime of the forest canopy.

The length of the growing season can be determined by using imaging radar data to monitor freeze/thaw transitions. At microwave frequencies freezing results in a large decrease of the dielectric constant of soil and vegetation because the crystal structure in frozen water prevents the rotation of the polar water molecules which they contain. Wegmuller and Werner (1995) attributed a 3-4 dB drop in radar backscatter from bare soils during day-night freeze-thaw cycles to this phenomenon. Backscatter change resulting from freezing and thawing was first

observed in image data in a series of L band aircraft radar data sets that were acquired over the Bonanza Creek Experimental Forest site near Fairbanks, Alaska, in 1988 (Way et al. 1990; Way et al. 1994).

The most recent study by Way et al. (1997) looked at ERS-1 Ice Phase data (3 day repeat) and used stem temperature to assess changes in backscatter. They found three distinct regimes:

i) below freezing, where backscatter is low and relatively constant;

ii) above freezing, where backscatter is higher and may reflect variations in the moisture status of the forest; and

iii) a transition from lower to higher values as different components of the ecosystem thaw (indicated by a range of stem temperatures which include values below zero, when canopy components thaw, to values above zero, when the soil thaws).

5 Forest canopy height

Because of the deeper penetration into the forest canopy at longer radar wavelengths, the interferometric effective height inferred from L-band and C-band SAR interferometry will constitute different fractions of the overall canopy height. Mean tree height in a pixel can therefore be inferred

i) from the height discontinuity at a boundary between a tree canopy and an adjacent cleared area;

ii) from the difference between the phase scattering centres as a function of wavelength;

iii) from the difference between the interferometric effective height from InSAR and a sufficiently accurate digital elevation model (DEM).

Sarabandi (1997) presented a study of the theoretical aspects of estimating vegetation parameters from SAR interferometry. The phase of the interferogram is proportional to the phase scattering centre of the target, and the coherence is inversely proportional to the uncertainty with which the phase can be estimated. For distributed targets such as a forest canopy the phase of the interferogram is a random variable which is a function of the system parameters and target scattering mechanisms. However, despite the complications arising from a three-dimensional array of scatterers, Sarabandi (1997) found that for a uniform closed canopy the extinction and the physical height of the canopy top could be estimated very accurately.

Hagberg et al. (1995) studied a dense boreal forest with InSAR. The interferometric height discontinuity at the forest to non-forest boundary showed good agreement with in-situ tree height measurements, although for a less dense forest the discontinuity was found to decrease, suggesting the possibility of estimating bole volume from the interferometric tree height and a ground DEM. Hagberg et al. (1995) also used the decrease of coherence over a dense forest with increasing baseline to estimate the effective scattering layer thickness.

Treuhaft et al. (1996) modelled the interferometric radar response to vegetation and topography. Four parameters were used to describe vegetation and topography: vegetation layer depth, vegetation extinction coefficient, a parameter involving the product of the average backscattering amplitude and scatterer number density, and the elevation of the ground. Their analysis of airborne InSAR data from Bonanza Creek Experimental Forest in Alaska showed approximately 5 m average ground truth agreement for vegetation layer depths and ground-surface heights, with a dependence of error on stand height.

The methods described above require precise estimates of the interferometric effective height. This precision crucially depends on sufficiently high coherence between the images.

Particularly at shorter wavelengths, decorrelation over forested areas can be high. At C- and X-band even light to moderate wind can cause a loss of coherence (Gray and Farrismanning 1993).

Askne et al. (1997) estimated the interferometric effective height of the forest by comparison of the InSAR height map with a digital elevation model. They also developed a model to relate basic forest properties to interferometric SAR observations, showing that the coherence and interferometric effective height change between image pairs. The model demonstrated how these properties are related to temporal decorrelation and to scattering from the vegetation canopy and the ground surface, and showed the important effect of gaps in the vegetation canopy. They inferred that the information content of the SAR backscatter intensity alone was limited, but that considerably more information about forest parameters could be derived if coherence and interferometric effective height could also be included.

Most published work on SAR interferometry uses a single-wavelength, single-polarization sensor. However, fully polarimetric SAR sensors, with both horizontal and vertical transmit and receive polarization, have been employed in the past and are being used at present, like the SIR-C mission or airborne sensors like JPL AIRSAR or the Danish EMISAR. If the baseline between repeated overflights is small enough, techniques of polarimetric SAR interferometry can be used to improve mapping capabilities. Cloude and Papathanassiou (1998) have published a pioneering paper on the theoretical background of polarimetry in SAR interferometry. They proposed a general formulation for vector wave interferometry, which includes conventional scalar interferometry as a special case. They show how interferograms between all possible linear combinations of polarization states can be formed, from any one of the linear polarization states (HH, HV, VH, VV) measured at time 1, and any one of these four polarization states at time 2 - e.g. HH1VV2. This approach revealed the strong polarization dependence of the interferometric coherence. Cloude and Papathanassiou

(1998) describe an algorithm for coherence maximisation and formulate a new coherent decomposition for polarimetric SAR interferometry that allows separation of the effective phase scattering centres of different scattering mechanisms. This analysis gives the height of the phase scattering centre for volume scattering in the tree crowns and for double-bounce scattering at the tree-trunks. Cloude and Papathanassiou (1998) introduced a scattering model for an elevated forest canopy to demonstrate the effectiveness of the algorithms and the importance of wave polarization for the physical interpretation of SAR interferograms. The potential of polarimetric SAR interferometry was investigated using results from fully polarimetric interferometric SIR-C data collected over the Selenga delta region at Lake Baikal, Russia. The scattering mechanisms in the forest, arising from different types of interactions at the ground, branches and canopy top, can be separated polarimetrically and located at different heights so that the phase differences at different polarizations can be interpreted as canopy height differences. Over the forested area near Lake Baikal these height differences were found to be around 20-30m, and the authors suggest a direct relationship to forest canopy height. A prerequisite for this analysis is significant canopy penetration so that a fully polarimetric SAR operating at L-band or at a longer wavelength is required.

An alternative approach to polarimetric interferometric SAR image analysis is the inversion of a microwave scattering model. Because the number of forest structural parameters is higher than the number of SAR parameters measured, such a model inversion is not straightforward, and multiple solutions may exist for a given set of observations. Lin and Sarabandi (1999) presented a fractal-based coherent scattering model of the polarimetric and interferometric response to forest as a function of incidence angle, tree density, tree height, trunk diameter, branching angle, wood moisture, soil moisture, and finer structural features. A genetic algorithm has been used to estimate the input parameters of a forest stand from a set of measured polarimetric and interferometric backscatter responses of the stand.

V Outlook

SAR interferometry, and particularly polarimetric SAR interferometry has the potential to operationally deliver three-dimensional structural information on the Earth's surface and its vegetation cover. The Japanese satellite ALOS will be the first spaceborne SAR mission carrying an L-band SAR capable of repeat-pass polarimetric interferometry. Other future missions are in earlier planning stages, like the German-British collaborative project InfoTerra / TerraSAR or the American LightSAR.

As a conclusion from this review of application of InSAR to forest mapping and monitoring, SAR interferometry can estimate biophysical variables of forest ecosystems on continental scales which could hardly be retrieved with other methods. These variables may have future applications in forest ecosystem models, models of the global carbon cycle and the impacts of global climate change, and will certainly prove useful in the efforts to monitor sustainable forest management with respect to the international commitments to the UN Biodiversity Convention.

VI References

Askne, J. I. H., Dammert, P. B. G., Ulander, L. M. H. and Smith, G. 1997: C-band repeat-pass

interferometric SAR observations of the forest. IEEE Transactions On Geoscience and Remote Sensing 35, 25-35.

Baker, J. R., Mitchell, P. L., Cordey, R. A., Groom, G. B., Settle, J. J. and Stileman, M. R. 1994: Relationships between physical characteristics and polarimetric radar backscatter for Corsican Pine stands in Thetford Forest, UK. International Journal of Remote Sensing 15, 2827-2849.

Baker, J. R. and Luckman, A. J. (1999, in press): Microwave observations of boreal forests in the NOPEX area of Sweden and a comparison with observations of a temperate plantation in the UK. Journal of Agricultural and Forest Meteorology

Bamler, R. and Hartl, P. 1998: Synthetic Aperture Radar interferometry. Inverse Problems 14, R1-R54.

Chang, A. T. C., Foster, J. L., Hall, D. K., Goodison, B. E., Walker, A. E., Metcalfe, J. R. and Harby, A. 1997: Snow parameters derived from microwave measurements during the BOREAS winter field campaign. Journal of Geophysical Research-Atmospheres 102, 29663-29671.

Christensen, E. L., Skou, N., Dall, J., Woelders, K. W., Jorgensen, J. H., Granholm, J. and Madsen, S. N. 1998: EMISAR: An absolutely calibrated polarimetric L- and C-band SAR. IEEE Transactions On Geoscience and Remote Sensing 36, 1852-1865.

Cloude, S. R. and Papathanassiou, K. P. 1998: Polarimetric SAR interferometry. IEEE Transactions On Geoscience and Remote Sensing 36, 1551-1565.

Coltelli, M., Fornaro, G., Franceschetti, G. et al. 1996: SIR-C/X-SAR multifrequency multipass interferometry: A new tool for geological interpretation. Journal of Geophysical Research-Planets 101, 23127-23148.

Costantini, M. 1998: A novel phase unwrapping method based on network programming. IEEE Transactions On Geoscience and Remote Sensing 36, 813-821.

Costantini, M., Farina, A. and Zirilli, F. 1999: A fast phase unwrapping algorithm for SAR interferometry. IEEE Transactions On Geoscience and Remote Sensing 37, 452-460.

Dammert, P. B. G., Askne, J. I. H. and Kuhlmann, S. 1999: Unsupervised segmentation of multitemporal interferometric SAR images. IEEE Transactions On Geoscience and Remote Sensing 37, 2259-2271.

Delia, S. and Biasutti, R. 1999: DESCW: PC software supporting remote sensing data. ESA Bulletin - European Space Agency 84-88.

Dobson, M. C., Ulaby, F. T., Letoan, T., Beaudoin, A., Kasischke, E. S. and Christensen, N. 1992: Dependence of radar backscatter on coniferous forest biomass. IEEE Transactions On Geoscience and Remote Sensing 30, 412-415.

Dutra, L. V. and Huber, R. 1999: Feature extraction and selection for ERS-1/2 InSAR classification. International Journal of Remote Sensing 20, 993-1016.

Faller, N. P. and Meier, E. H. 1995: First results with the airborne single-pass Do-SAR interferometer. IEEE Transactions On Geoscience and Remote Sensing 33, 1230-1237.

Fornaro, G. and Franceschetti, G. 1995: Image registration in interferometric SAR processing. Iee Proceedings-Radar Sonar and Navigation 142, 313-320.

Fornaro, G., Franceschetti, G. and Lanari, R. 1996: Interferometric SAR phase unwrapping using Green's formulation. IEEE Transactions On Geoscience and Remote Sensing 34, 720-727.

Fornaro, G., Franceschetti, G., Lanari, R., Rossi, D. and Tesauro, M. 1997a: Interferometric SAR phase unwrapping using the finite element method. IEE Proceedings-Radar Sonar and Navigation 144, 266-274.

Fornaro, G., Franceschetti, G., Lanari, R., Sansosti, E. and Tesauro, M. 1997b: Global and local phase-unwrapping techniques: a comparison. Journal of the Optical Society of America A - Optics Image Science and Vision 14, 2702-2708.

Fornaro, G. and Sansosti, E. 1999: A two-dimensional region growing least squares phase unwrapping algorithm for interferometric SAR processing. IEEE Transactions On Geoscience and Remote Sensing 37, 2215-2226.

Freeman, A. 1992: SAR calibration - an overview. IEEE Transactions On Geoscience and Remote Sensing 30, 1107-1121.

Gelautz, M., Leberl, F. and Kellerer-Pirklbauer, W. 1996: Image enhancement and evaluation: SAR layover and shadows. AEU-Archiv für Elektronik und Übertragungstechnik-International Journal of Electronics and Communications 50, 100-105.

Gens, R. and VanGenderen, J. L. 1996: SAR interferometry - Issues, techniques, applications. International Journal of Remote Sensing 17, 1803-1835.

Goldstein, R. M. and Werner, C. L. 1998: Radar interferogram filtering for geophysical applications. Geophysical Research Letters 25, 4035-4038.

Goyal, R. K. and Verma, A. K. 1996: Mathematical formulation for estimation of baseline in synthetic aperture radar interferometry. Sadhana-Academy Proceedings in Engineering Sciences 21, 511-522.

Gray, A. L. and Farrismanning, P. J. 1993: Repeat-pass interferometry with airborne Synthetic Aperture Radar. IEEE Transactions On Geoscience and Remote Sensing 31, 180-191.

Griffiths, H. D. and Wilkinson, A. J. 1994: Improvements in phase unwrapping algorithms for interferometric SAR. Onde Electrique 74, 46-52.

Hagberg, J. O., Ulander, L. M. H. and Askne, J. 1995: Repeat-pass SAR interferometry over forested terrain. IEEE Transactions On Geoscience and Remote Sensing 33, 331-340.

Hilland, J. E., Stuhr, F. V., Freeman, A., Imel, D., Shen, Y., Jordan, R. L. and Caro, E. R. 1998: Future NASA spaceborne SAR missions. IEEE Aerospace and Electronic Systems Magazine 13, 9-16.

Imhoff, M. L. 1995: Radar backscatter and biomass saturation - Ramifications for global biomass inventory. IEEE Transactions On Geoscience and Remote Sensing 33, 511-518.

Just, D. and Bamler, R. 1994: Phase statistics of interferograms with applications to Synthetic Aperture Radar. Applied Optics 33, 4361-4368.

Kasischke, E. S., Melack, J. M. and Dobson, M. C. 1997: The use of imaging radars for ecological applications - A review. Remote Sensing of Environment 59, 141-156.

Lee, J. S., Hoppel, K. W., Mango, S. A. and Miller, A. R. 1994: Intensity and phase statistics of multilook polarimetric and interferometric SAR imagery. IEEE Transactions On Geoscience and Remote Sensing 32, 1017-1028.

Lee, J. S., Papathanassiou, K. P., Ainsworth, T. L., Grunes, M. R. and Reigber, A. 1998: A new technique for noise filtering of SAR interferometric phase images. IEEE Transactions On Geoscience and Remote Sensing 36, 1456-1465.

Lin, Q., Vesecky, J. F. and Zebker, H. A. 1992: New approaches in interferometric SAR data processing. IEEE Transactions On Geoscience and Remote Sensing 30, 560-567.

Lin, Y. C. and Sarabandi, K. 1999: Retrieval of forest parameters using a fractal-based coherent scattering model and a genetic algorithm. IEEE Transactions On Geoscience and Remote Sensing 37, 1415-1424.

Luckman, A., Baker, J., Honzak, M. and Lucas, R. 1998: Tropical forest biomass density estimation using JERS-1 SAR: Seasonal variation, confidence limits, and application to image mosaics. Remote Sensing of Environment 63, 126-139.

Lyuboshenko, I. and Maitre, H. 1999: Phase unwrapping for interferometric synthetic aperture radar by use of Helmholtz equation eigenfunctions and the first Green's identity. Journal of the Optical Society of America A - Optics Image Science and Vision 16, 378-395.

Madsen, S. N., Martin, J. M. and Zebker, H. A. 1995: Analysis and evaluation of the NASA/JPL TOPSAR across-track interferometric SAR system. IEEE Transactions On

Geoscience and Remote Sensing 33, 383-391.

Madsen, S. N., Zebker, H. A. and Martin, J. 1993: Topographic mapping using radar interferometry - Processing techniques. IEEE Transactions On Geoscience and Remote Sensing 31, 246-256.

Moghaddam, M. and Saatchi, S. 1995: Analysis of scattering mechanisms in SAR imagery over boreal forest - Results from BOREAS-93. IEEE Transactions On Geoscience and Remote Sensing 33, 1290-1296.

Pritt, M. D. 1996: Phase unwrapping by means of multigrid techniques for interferometric SAR. IEEE Transactions On Geoscience and Remote Sensing 34, 728-738.

Ranson, K. J., Saatchi, S. and Sun, G. Q. 1995: Boreal forest ecosystem characterization with SIR-C/X-SAR. IEEE Transactions On Geoscience and Remote Sensing 33, 867-876.

Ranson, K. J., Sun, G. Q., Lang, R. H., Chauhan, N. S., Cacciola, R. J. and Kilic, O. 1997: Mapping of boreal forest biomass from spaceborne Synthetic Aperture Radar. Journal of Geophysical Research-Atmospheres 102, 29599-29610.

Rignot, E. 1996: Dual-frequency interferometric SAR observations of a tropical rain- forest. Geophysical Research Letters 23, 993-996.

Rosen, P. A., Hensley, S., Zebker, H. A., Webb, F. H. and Fielding, E. J. 1996: Surface deformation and coherence measurements of Kilauea volcano, Hawaii, from SIR-C radar interferometry. Journal of Geophysical Research-Planets 101, 23109-23125.

Rossi, M., Rogron, B. and Massonnet, D. 1996: JERS-1 SAR image quality and interferometric potential. IEEE Transactions On Geoscience and Remote Sensing 34, 824-827.

Rufino, G., Moccia, A. and Esposito, S. 1998: DEM generation by means of ERS tandem data. IEEE Transactions On Geoscience and Remote Sensing 36, 1905-1912.

Sarabandi, K. 1997: Delta k-radar equivalent of interferometric SAR's: A theoretical study for

determination of vegetation height. IEEE Transactions On Geoscience and Remote Sensing 35, 1267-1276.

Tough, R. J. A., Blacknell, D. and Quegan, S. 1995: A statistical description of polarimetric and interferometric Synthetic-Aperture Radar data. Proceedings of the Royal Society of London Series A - Mathematical and Physical Sciences 449, 567-589.

Treuhaft, R. N., Madsen, S. N., Moghaddam, M. and van Zyl, J. J. 1996: Vegetation characteristics and underlying topography from interferometric radar. Radio Science 31, 1449-1485.

Trouve, E., Nicolas, J. M. and Maitre, H. 1998: Improving phase unwrapping techniques by the use of local frequency estimates. IEEE Transactions On Geoscience and Remote Sensing 36, 1963-1972.

Ulander, L. M. H. 1996: Radiometric slope correction of Synthetic Aperture Radar images. IEEE Transactions On Geoscience and Remote Sensing 34, 1115-1122.

Wang, Z. J. and Li, S. S. 1999: Phase unwrapping through a branch-cut-based cut-bridging and window- patching method. Applied Optics 38, 805-814.

Way, J., Paris, J., Kasischke, E. et al. 1990: The effect of changing environmental conditions on microwave signatures of forest ecosystems - Preliminary results of the March 1988 Alaskan aircraft SAR experiment. International Journal of Remote Sensing 11, 1119-1144.

Way, J., Rignot, E. J. M., McDonald, K. C., Oren, R., Kwok, R., Bonan, G., Dobson, M. C., Viereck, L. A. and Roth, J. E. 1994: Evaluating the type and state of Alaska taiga forests with imaging radar for use in ecosystem models. IEEE Transactions On Geoscience and Remote Sensing 32, 353-370.

Way, J., Zimmermann, R., Rignot, E., McDonald, K. and Oren, R. 1997: Winter and spring thaw as observed with imaging radar at BOREAS. Journal of Geophysical Research-Atmospheres 102, 29673-29684.

Wegmuller, U. and Werner, C.L. 1995: SAR interferometric signatures of forest. IEEE Transactions On Geoscience and Remote Sensing 33, 1153-1161.

Wegmuller, U. and Werner, C. 1997: Retrieval of vegetation parameters with SAR interferometry. IEEE Transactions On Geoscience and Remote Sensing 35, 18-24.

Xu, W. and Cumming, I. 1999: A region-growing algorithm for InSAR phase unwrapping. IEEE Transactions On Geoscience and Remote Sensing 37, 124-134.

Zebker, H. A., Farr, T. G., Salazar, R. P. and Dixon, T. H. 1994a: Mapping the worlds topography using radar interferometry - the Topsat Mission. Proceedings of the IEEE 82, 1774-1786.

Zebker, H. A., Werner, C. L., Rosen, P. A. and Hensley, S. 1994b: Accuracy of topographic maps derived from ERS-1 interferometric radar. IEEE Transactions On Geoscience and Remote Sensing 32, 823-836

Zebker, H. A. and Lu, Y. P. 1998: Phase unwrapping algorithms for radar interferometry: Residue-cut, least-squares, and synthesis algorithms. Journal of the Optical Society of America A - Optics Image Science and Vision 15, 586-598.

Zebker, H. A., Rosen, P. A. and Hensley, S. 1997: Atmospheric effects in interferometric Synthetic Aperture Radar surface deformation and topographic maps. Journal of Geophysical Research-Solid Earth 102, 7547-7563.

Zebker, H. A. and Villasenor, J. 1992: Decorrelation in interferometric radar echoes. IEEE Transactions On Geoscience and Remote Sensing 30, 950-959.

Tables, figures and images

Table 1: Past, present and planned orbital SAR missions.

Satellite	launch date	freq (GHz)	band	polari-zations	resolu-tion (m)	swath width (km)	look angle (deg)	inciden-ce angle (deg)	repeat cycle (days)
ERS-1	6/1991	5.25	C	VV	30	100	20	23-35	3, 35, 168
JERS-1	summer 1992	1.28	L	HH	18	75	35	38	44
SIR-C	4/1994 & 10/1/ 1994	1.25, 5.3	L, C	HH, VV, HV (quad.)	10-40	15-90	15-55		(1)
ERS-2	spring 1995	5.25	C	VV	30	100	20	23-35	(1), 35
Radarsat	10/ 1995	5.3	C	HH	10-100	45-500	20-59		(2-3)
Envisat	2000	5.25	C	HH, VV, HV (not quad.)					35
ALOS	2002	1.28	L	HH, VV, HV (experi-mental quad-pol mode)					45

Figures and images

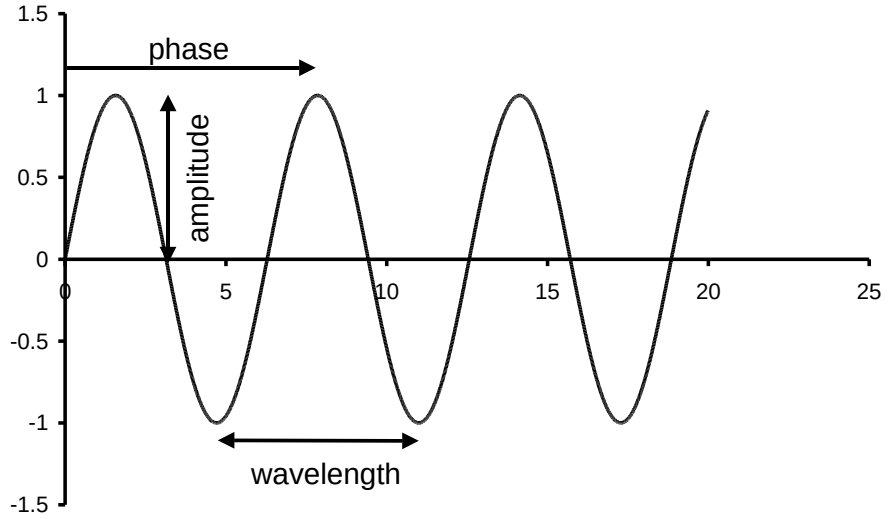

Figure 1: Amplitude, phase and wavelength of a radar signal. The intensity of the signal is the squared amplitude.

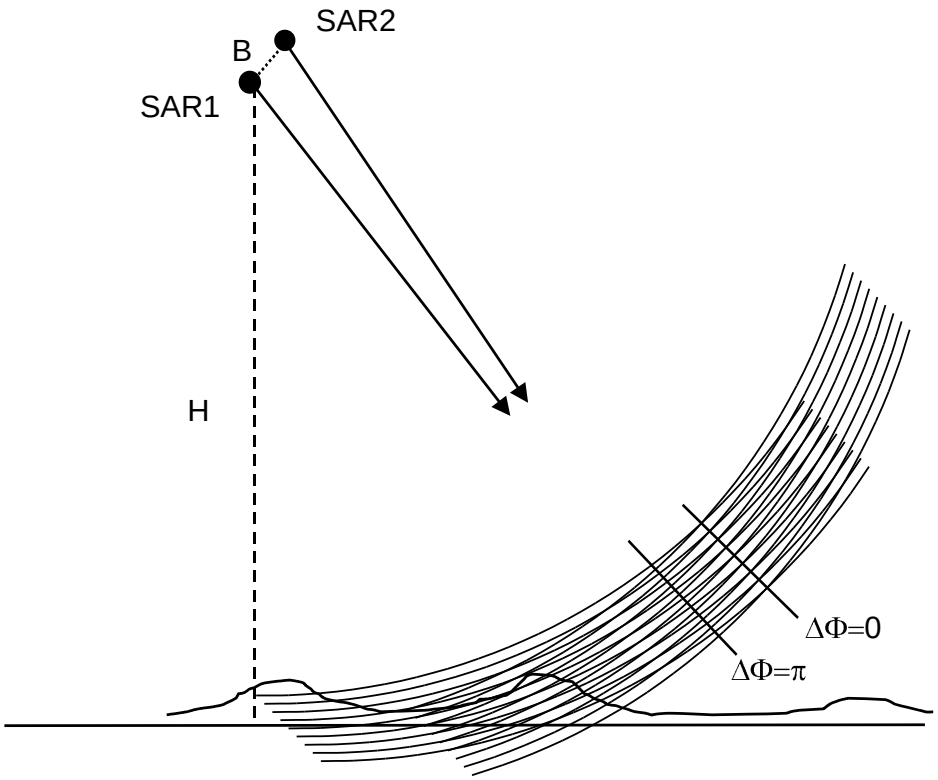

Figure 2: Interference of iso-phase lines of two SAR sensors separated by a spatial baseline B. The distance between two iso-phase lines is half the wavelength. The absolute phase difference $\Delta\Phi$ fluctuates between 0 and π, as indicated by the two orthogonal lines.